Geochemical Perspectives Letters

Emergence of peraluminous crustal magmas and implications for the early Earth

M.R. Ackerson, D. Trail, J. Buettner

Supplementary Information

The Supplementary Information includes:

- Extended Methods
- Supplementary Tables S-1 and S-2
- Supplementary Figures S-1 through S-8
- Supplementary Information References

Extended Methods

Whole rock samples were crushed to a sand using a BICO chipmunk jaw crusher with steel plates followed by a BICO pulveriser fitted with alumina disks. The resulting sand was screened using a water wash step to remove clays and fine particles, passed with a hand magnet to remove magnetic particles, and was run through a Frantz magnetic separator. Finally, methylene iodide was used to procure a concentrated zircon separate.

Zircons separates were mounted in epoxy and polished through their cores using successive 3 and 1 µm SiC lapping film, followed by 0.1 µm Type A diamond lapping film and a final polish using colloidal silica to flatten the surface of the zircons. Several epoxy mounts were also treated with an additional weak hydrofluoric acid surface treatment to facilitate dissolution of inclusions and metamict regions within zircons. While not necessary for quality analyses, this step did generally produce a higher proportion of clean laser ablation analyses than non-treated samples. Prior to analyses, each zircon was inspected in optical and transmitted light to ensure that analytical spots were not placed on metamict regions of zircons or on inclusions.

Sectioned zircons were analysed on an Agilent 7900 quadrupole inductively coupled plasma mass spectrometer (ICPMS) at the University of Rochester, fitted with a Cetac (Photon Machines) Analyte G2 193 nm laser ablation (LA) unit with a HelEx 2 volume chamber sample cell. Trace element data was collected with a 20 µm circular spot for analytical durations of 20 s with a 7 Hz pulse rate and a laser energy of 6.75 J/cm^2 (Wang and Trail, 2019). The number of masses analysed was minimised in order to increase the signal for the masses of primary interest. Masses analysed include: ^{7}Li, ^{23}Na, ^{24}Mg, ^{27}Al, ^{31}P, ^{49}Ti, ^{57}Fe, ^{146}Nd, ^{147}Sm, ^{163}Dy, ^{204}Pb, ^{206}Pb, and ^{207}Pb (see Supplementary Table S-2).

Zircon U-Pb ages were determined following similar procedures to those described in Trail *et al*. (2017) Epoxy mounts were loaded into the HelEx 2 volume chamber and the He flow was set to 0.6 L/min in the chamber, and 0.2 L/min in the HelEx arm. The laser energy was set to 7 mJ (fluence = 11.8 J/cm^2), with a pulse rate of 10 Hz. A circular spot of 25 µm was selected for all analyses. For each analysis, background counts were collected first (~30 s), followed by 20 s of ablation, and then a 30 s washout period before moving on to the next zircon. Zircon ages were standardised against the AS-3 geochronology standard (Paces and Miller, 1993), and also monitored with a secondary in-house

standard, Kuehl Lake, believed to be from the same locality as the international zircon standard 91500 (Trail *et al*., 2018). We analysed ^{202}Hg, ^{204}Pb, ^{206}Pb, ^{207}Pb, ^{208}Pb, ^{232}Th, and ^{238}U. The integration times for ^{206}Pb and ^{207}Pb were set at 30 ms, and those for the other isotopes were set at 10 ms for each cycle. All data reduction, and correction for downhole Pb-U fractionation was done with the Iolite 3.32 software package (Paton *et al*., 2018).

After chemical analyses, select zircons were also imaged using the panchromatic cathodoluminescence (CL) detector on the JEOL 8530F electron probe microanalyser (EPMA) at the Smithsonian Institution (Fig. S-1) in order to observe internal chemical zonation and to ensure that both age and chemistry laser spots targeted similar regions of the zircon.

Obtaining primary Al concentrations from the zircons was one of the main goals of this study. Al is known to be a contaminant in zircon analyses and is often used to monitor contamination in SIMS analysis (Piazolo *et al*., 2016; Lyon *et al*., 2019). Therefore, care was taken to ensure the filtering techniques described above eliminate non-primary Al measurements from consideration. There has been some discussion in the literature over the precise value of LREE index to use for filtering zircon compositions (Bell *et al*., 2019). In our sample set, filtering of data for Fe and discordance prior to LREE-I filtering results in similar results, regardless of the LREE filter occurring at 30 or 50 (Fig. S-3).

Supplementary Tables

Table S-1 Sampling locations for metasedimentary rocks of the Jack Hills presented in this study.

Sample	Easting	Northing
T136	499199	7106296
T139	499207	7106283
T140	499193	7106279
T145	499235	7106170
T146	499231	7106157
T147	499245	7106139
T148	499253	7106125
T152	499274	7106030

Table S-2 Sample numbers, ages, and chemical information for individual zircon crystals within the Jack Hills metamorphic belt.

The data table is available for download (Excel file) at https://www.geochemicalperspectivesletters.org/article2114.

Supplementary Figures

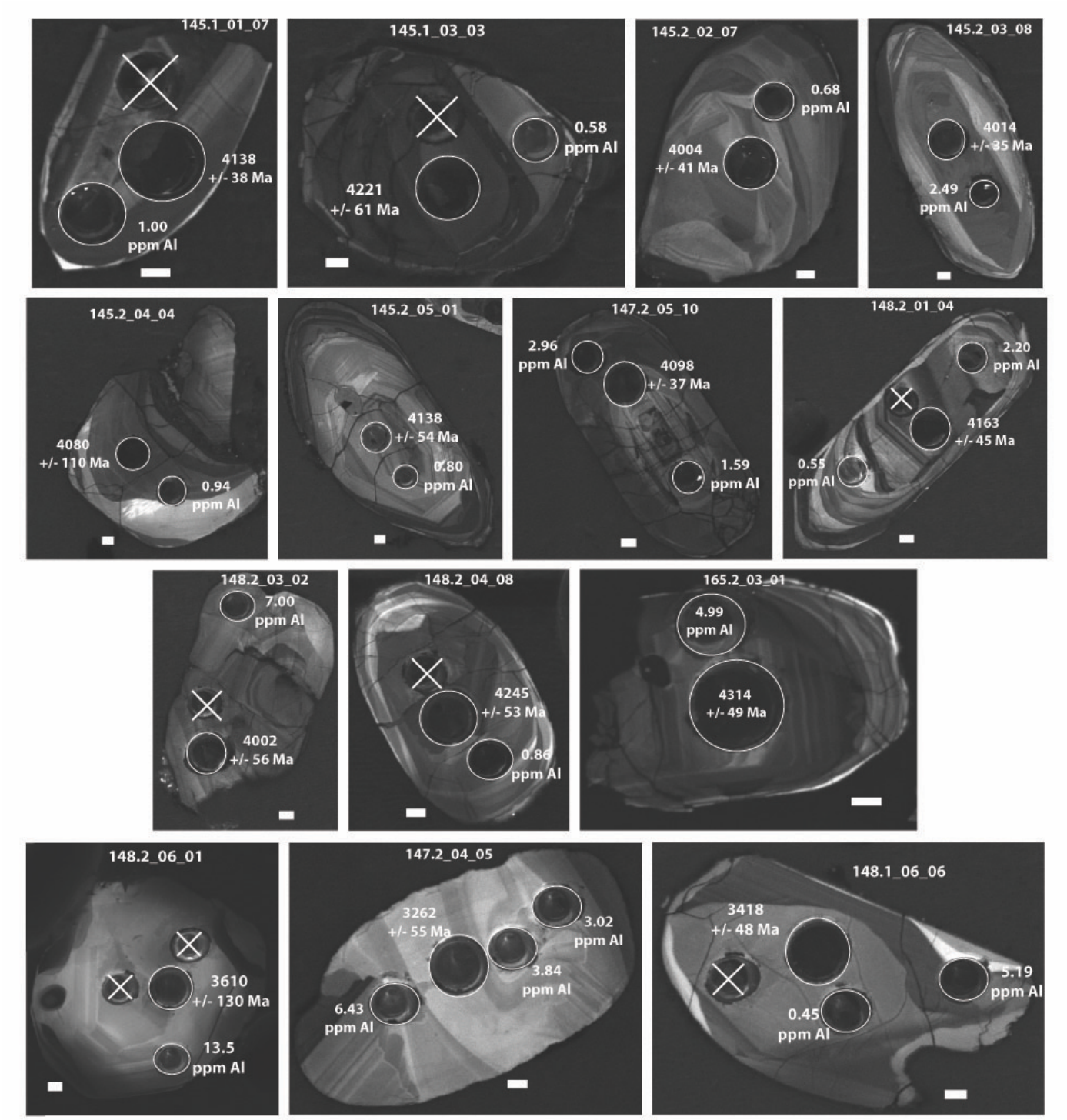

Figure S-1 Cathodoluminescence images of select Hadean and/or likely peraluminous zircons from the Jack Hills greenstone belt. 25 µm spots were used for dating, and 20 µm spots were used for chemical analyses. Reported errors on ages are 2σ. Scale bars are 10 µm.

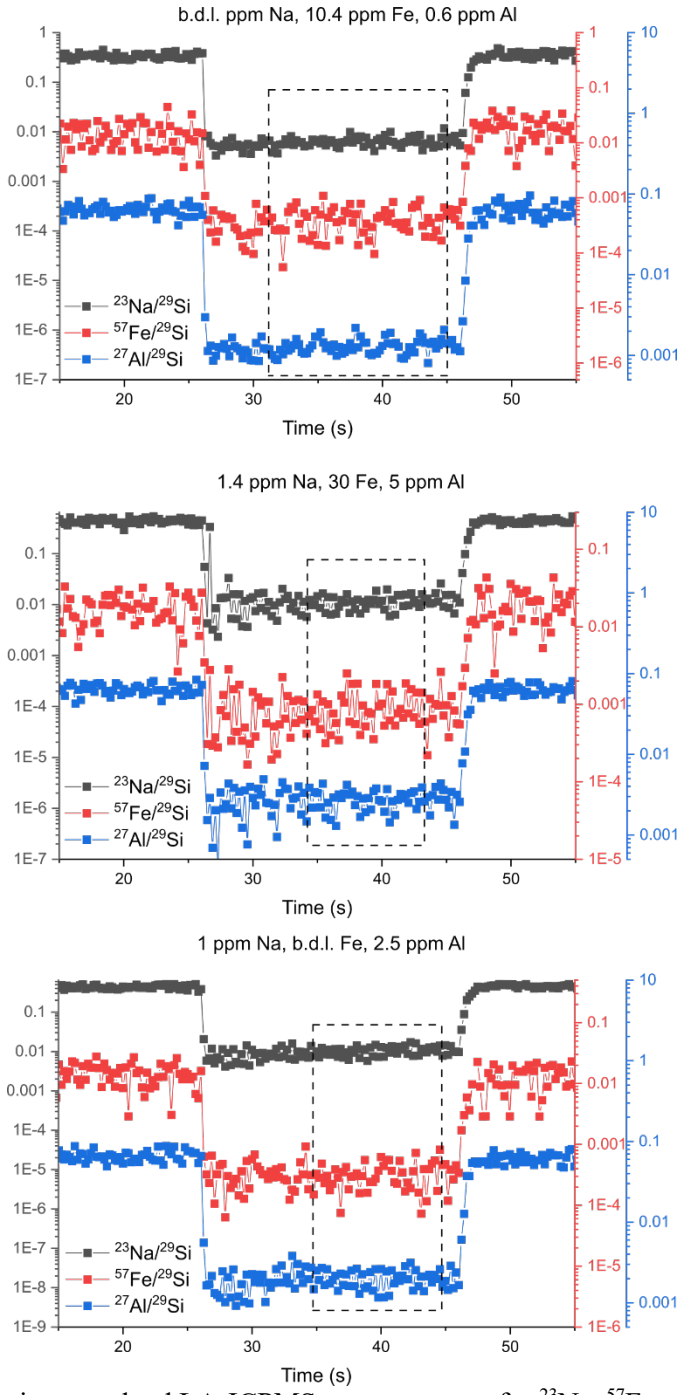

Figure S-2 Representative time-resolved LA-ICPMS measurements for ^{23}Na, ^{57}Fe and ^{27}Al relative to ^{29}Si. Dashed boxes are the analytical window used to calculate trace element concentrations in the zircons. Care was taken to avoid regions of the time-resolved spectra that contained ephemeral spikes in elements that are likely caused by laser pits ablating impurities during analysis.

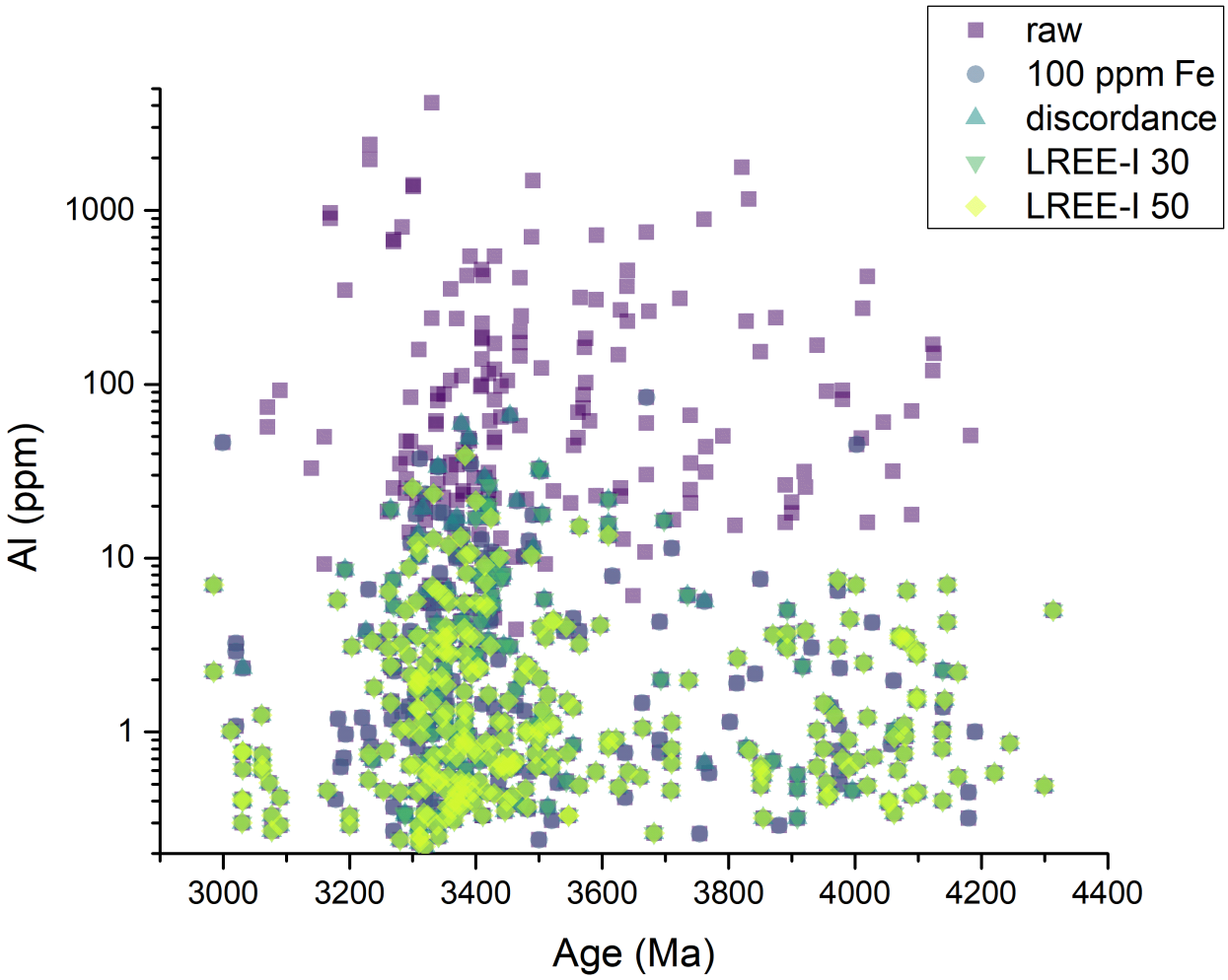

Figure S-3 Age versus X_{Al}^{Zrc} for JH zircons showing the change in population as a function of the filtering steps applied, including both the LREE-I 30 (Bell *et al.*, 2016) and LREE-I 50 filters (Bell *et al.*, 2019).

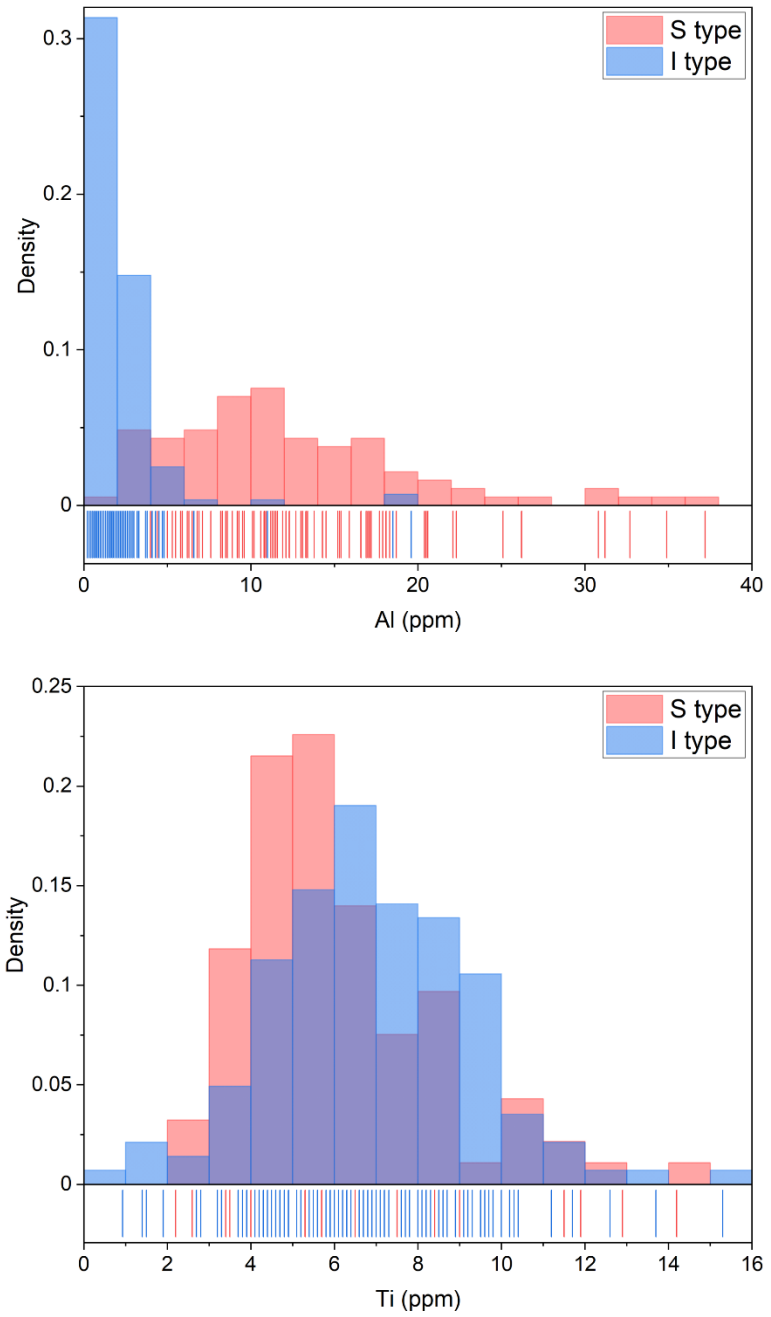

Figure S-4 Ti and Al concentrations in granitoid-hosted zircons from the Lachlan Fold Belt (LFB, Trail *et al.*, 2017), showing the dominant role of melt composition over temperature in regulating Al content in zircons in the LFB. As a proxy for temperature, Ti content in S-type zircons is similar to that of I-type zircons, indicating similar crystallization temperatures. However, S-type zircons crystallised from moderately to strongly peraluminous melts contain higher Al concentrations.

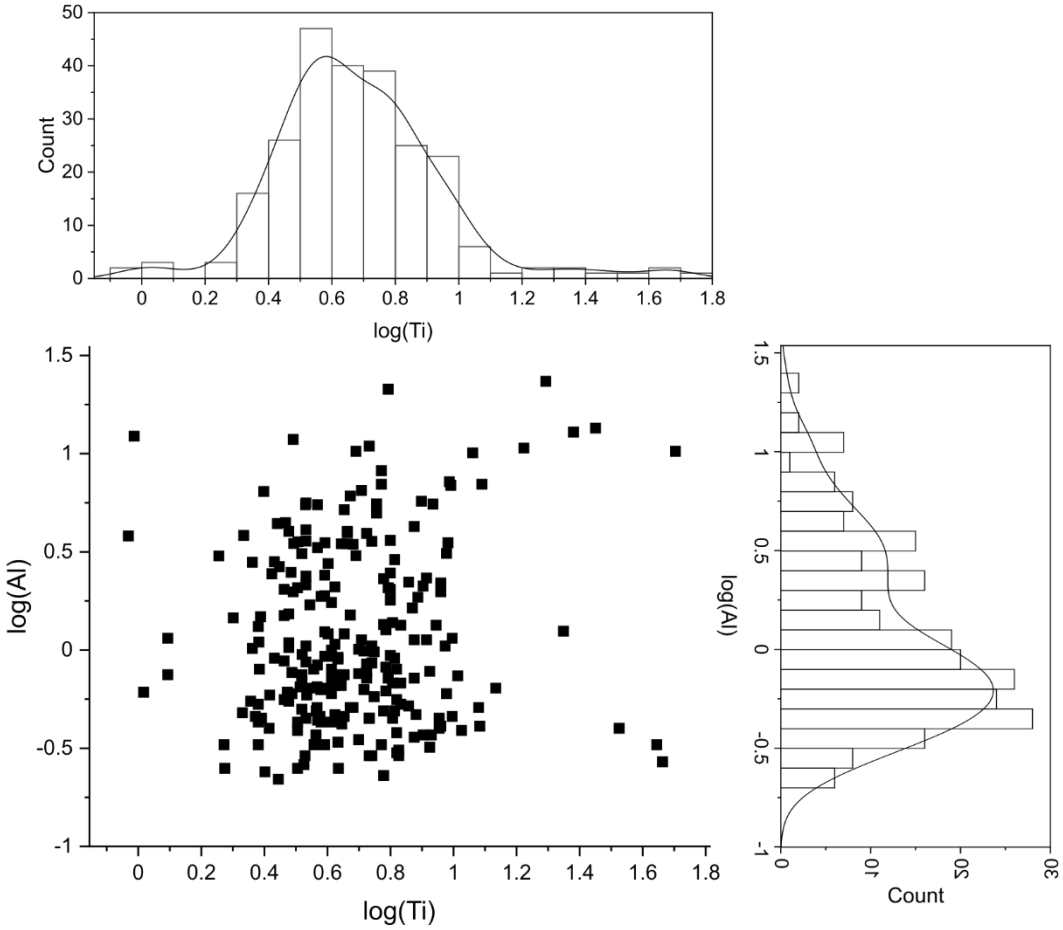

Figure S-5 Ti and Al concentrations in zircons from the Jack Hills, with little evidence of correlation between Ti (proxy for temperature) and Al content.

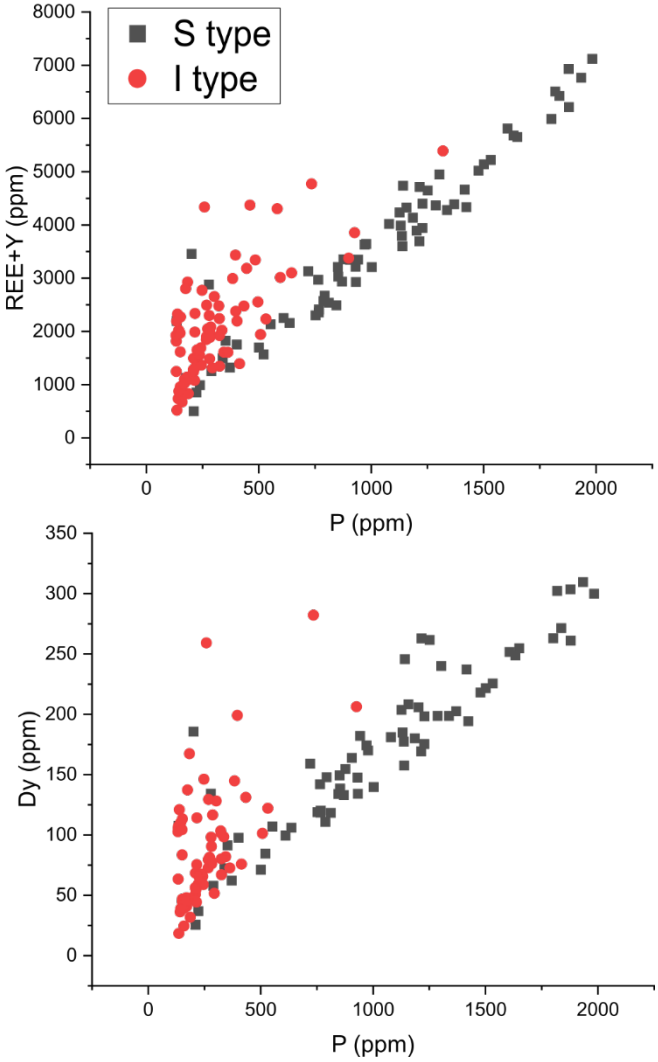

Figure S-6 Comparison of P-Dy and P-REE+Y plots, showing broad similarity between the two plots. Dy is used in thus study as a proxy for the a total REE plot (Burnham and Berry, 2017) as only a limited number of elements were analysed in the present study to maximise the signal from elements of interest during analysis.

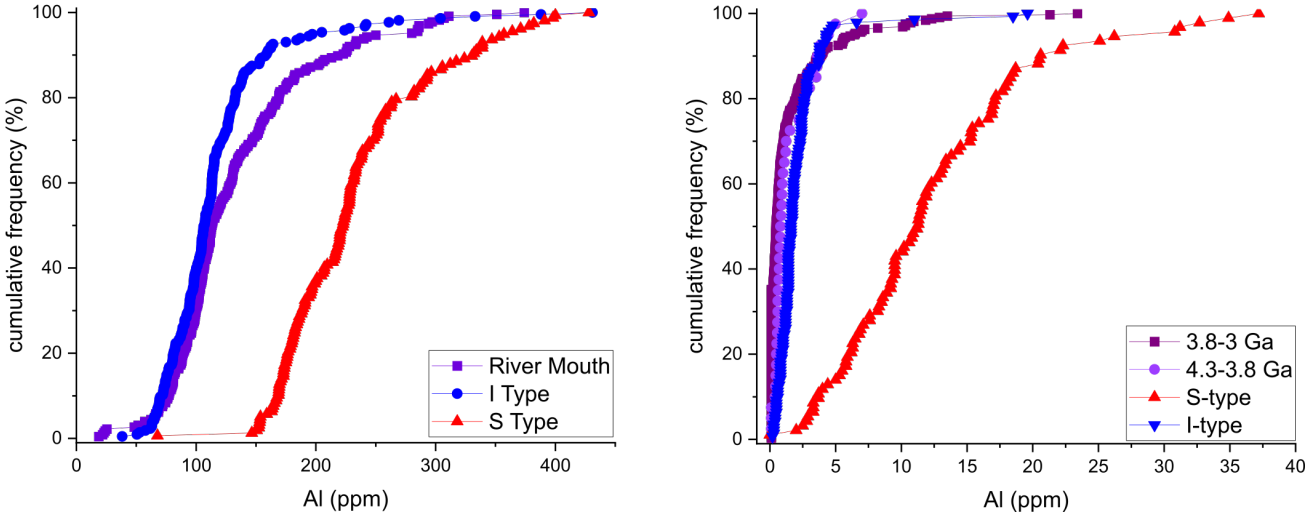

Figure S-7 **(Left)** Al concentrations in quartz grains from sediments at the mouth of the Bega River, NSW, Australia compared with regional bedrock I- and S-type granitoids, showing mixed I- and S-type signals in the sediments that reflect the diversity of bedrock in the region (Ackerson *et al.*, 2015). **(Right)** JH zircons show a similar mixing between peraluminous and non-peraluminous sources, starting noticeably in the 3.5-3 Ga bin.

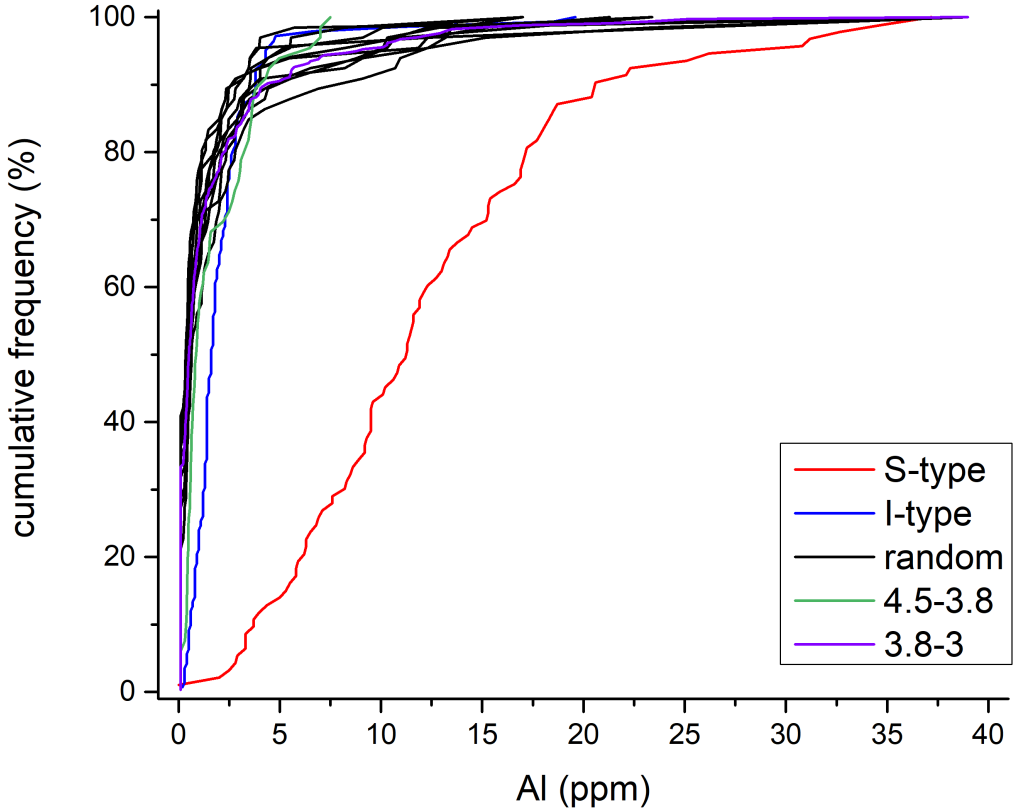

Figure S-8 Random subsampling of 3.5-3 Ga JH zircons. The large number of zircons from the 3.8-3 Ga bin (n = 332) compared to the 4.5-3.8 Ga (n = 66) makes it is possible that peraluminous signal in the Hadean-aged bin may have been missed by the limited number of Hadean-aged zircons measured. The 3.8-3 Ga bin was randomly subsampled to n = 66 zircon populations as a test of sample-number bias. At the 95 % confidence level using a Kolmogorov-Smirnov Test, only 1 of the 10 random subsamples was statistically similar to the 4.5-3.8 Ga bin, whereas all random subsamples were statistically similar to the 3.8-3 Ga bin. This suggests it is unlikely that under-sampling of the Hadean population failed to record a peraluminous signature.

Supplementary Information References

Ackerson, M.R., Tailby, N.D., Watson, E.B. (2015) Trace elements in quartz shed light on sediment provenance. *Geochemistry, Geophysics, Geosystems* 16, 1894–1904.

Bell, E.A., Boehnke, P., Harrison, T.M. (2016) Recovering the primary geochemistry of Jack Hills zircons through quantitative estimates of chemical alteration. *Geochimica et Cosmochimica Acta* 191, 187–202.

Bell, E.A., Boehnke, P., Barboni, M., Harrison, T.M. (2019) Tracking chemical alteration in magmatic zircon using rare earth element abundances. *Chemical Geology* 510, 56–71.

Burnham, A.D., Berry, A.J. (2017) Formation of Hadean granites by melting of igneous crust. *Nature Geoscience* 10, 457–461.

Lyon, I.C., Kusiak, M.A., Wirth, R., Whitehouse, M.J., Dunkley, D.J., Wilde, S.A., Schaumlöffel, D., Malherbe, J., Moore, K.L. (2019) Pb nanospheres in ancient zircon yield model ages for zircon formation and Pb mobilization. *Scientific Reports* 9, 1–9.

Paces, J.B., Miller, J.D. (1993) Precise U-Pb ages of Duluth Complex and related mafic intrusions, northeastern Minnesota: Geochronological insights to physical, petrogenetic, paleomagnetic, and tectonomagmatic processes associated with the 1.1 Ga Midcontinent Rift System. *Journal of Geophysical Research: Solid Earth* 98, 13997–14013.

Paton, C., Woodhead, J.D., Hellstrom, J.C., Hergt, J.M., Greig, A., Maas, R. (2018) Improved laser ablation U-Pb zircon geochronology through robust downhole fractionation correction. *Geochemistry, Geophysics, Geosystems* 11, Q0AA06.

Piazolo, S., La Fontaine, A., Trimby, P., Harley, S., Yang, L., Armstrong, R., Cairney, J.M. (2016) Deformation-induced trace element redistribution in zircon revealed using atom probe tomography. *Nature Communications* 7, 1–7.

Trail, D., Tailby, N., Wang, Y., Harrison, T.M., Boehnke, P. (2017) Aluminum in zircon as evidence for peraluminous and metaluminous melts from the Hadean to present. *Geochemistry, Geophysics, Geosystems* 18, 1580–1593.

Trail, D., Boehnke, P., Savage, P.S., Liu, M.-C., Miller, M.L., Bindeman, I. (2018) Origin and significance of Si and O isotope heterogeneities in Phanerozoic, Archean, and Hadean zircon. *Proceedings of the National Academy of Sciences* 115, 10287–10292.

Wang, Y., Trail, D. (2019) Aluminum partitioning between zircon and haplogranitic melts: The influence of temperature and melt composition. *Chemical Geology* 511, 71–80.